OPEN ACCESS

University of Dundee

University of Dundee

Passivating effect of ternary alloyed AgZnSe shell layer on the structural and luminescent properties of CdS quantum dots

Adegoke, Oluwasesan; Montaseri, Hanieh; Nsibande, Sifiso A.; Forbes, Patricia B.C.

Passivating effect of ternary alloyed AgZnSe shell layer on the structural and luminescent properties of CdS quantum dots

Oluwasesan Adegoke, Hanieh Montaseri, Sifiso A. Nsibande, Patricia B.C. Forbes *

Department of Chemistry, Faculty of Natural and Agricultural Sciences, University of Pretoria, Lynnwood Road, Pretoria 0002, South Africa

*Corresponding author: *Email address:* adegoke.sesan@mailbox.co.za (O. Adegoke), patricia.forbes@up.ac.za (P.B.C. Forbes)

Abstract

The surface passivation of luminescent CdS quantum dots (QDs) via epitaxial overgrowth of new alloyed ternary AgZnSe shell layer is reported here. Two synthetic fabrication strategies were used to tune the optical properties of CdS/AgZnSe core/alloyed shell QDs across the visible region. Transmission electron microscopy, powder X-ray diffraction, Raman, UV/vis and fluorescence spectrophotometric techniques were used to characterize the nanocrystals. Analysis of the internal structure of the QDs revealed that homogeneity of the particle reduced as the size increased, thus indicating that the QDs growth transitioned from an interfacial epitaxial homogenous state to a heterogeneous state. The crystal structure of the QDs revealed a distinct zinc-blende diffraction pattern for CdS while CdS/AgZnSe core/alloyed shell QDs kinetically favoured a phase change process from the zinc-blende phase to a wurtzite phase. Analysis of the photophysical properties revealed varying degrees of interfacial defect state suppression in CdS/AgZnSe QDs which was dependent on the QDs size. Specifically, the fluorescence quantum yield (QY) of CdS/AgZnSe QDs was at most ~5-fold higher than the CdS core and varied from 35-73%. We found that band gap modulation via the synthetic fabrication strategy employed, influenced the optical properties of the core/alloyed shell QDs. The CdS/AgZnSe QDs produced in this work hold great promise in light-emitting optoelectronic applications.

1. Introduction

The wide electro-luminescent applications of colloidal semiconductor quantum dot (QD) nanocrystals in various fields of chemistry, biology and physics, stem from their unique optoelectronic properties [1,2]. Particularly, the size-dependent optical and electronic properties of QDs which are governed by the associated quantum confinement feature, allows tuning of the photoluminescence (PL) emission from the ultraviolet/visible (UV/vis) region to the far infra-red region [3-6]. In contrast to bulk semiconductors in which the surface represents a tiny fraction of the bulk material, colloidal QDs have their size typically in the range of 2–10 nm. This unique characteristic enables a large number of atoms to be embedded on the QD surface [7].

The QD surface represents a highly sensitive region that is exposed to its surrounding environment (matrices, solvents and various other species in solution) and it is typically coordinated by chemical ligands, surfactants or stabilizers that influence the QD optoelectronic properties [7]. The synergistic effects of precursor material which create low numbers of coordinated surface atoms may lead to highly reactive or localized electronic sites that are susceptible to redox and chemical processes. Thus, it is very likely for midgap, shallow or deep surface defect states to be formed and induce the pathway for poor PL properties. The characteristic phenomenon is nonradiative recombination exciton (electron and hole) states associated with low PL quantum yield (QY) [8,9]. One of the widely used strategies to eliminate surface traps is to passivate the QD core surface with a wider band gap shell material [10-13]. This strategy shifts the surface defects to the outer domain of the shell layer, thus improving the PL QY [4]. The electron and hole being localized in the core, represents a signature process associated with the low probability of the outer surface state being subjected to trapped photogenerated charge carriers [14,15].

69 Over the past two decades, the most studied class of semiconductor QDs are the group II-VI metal

70 chalcogenides with CdSe-based QDs being the most popular for fabricating new synthetic routes

71 [16], shell passivation [17], ligand dynamics [18] and alloying [19]. On the other hand, CdS

72 nanocrystals are probably the second most studied QD system [20-23], exhibiting an exciton Bohr

73 radius of 3.0 nm [24] and a bulk band gap of 2.48 eV [25]. Its characteristic PL emission is known

74 to be highly prone to surface defects which results in low PL QY [26]. Nonetheless, it is widely

75 used as a shell layer to overcoat the surface of CdSe-based QDs. The well-known strategy to isolate

76 the exciton wave function from the surface of the core QDs with embedded surface defects and

77 dangling bonds is to coat with a shell layer of a wide band gap [27]. However, it is important to

78 note that lattice mismatch between the core and binary shell material at the interface can also

79 induce surface defects that degrade the luminescence of the core/shell QDs, thus lowering the PL

80 QY [28].

81 Another strategy which has drawn significant interest in improving the PL QY of binary core QDs

82 is to coat the surface with an alloyed ternary shell layer. Alloyed QDs (AB_xC_{1-x}) have become

83 important in mainstream nanoscale optical engineering due to the added degree of freedom in

84 tuning the exciton energy for either extended PL emission range or improved optical properties

85 [29-32]. The coating of an alloyed ternary shell around binary core QDs to improve the PL

86 efficiency has mostly been reported for CdSe-based QDs [33,34] with rare reports for CdS-based

87 QDs [13]. It is noteworthy that apart from the formation of a smooth gradient band gap, the lattice

88 strain of the core/shell QDs can be relaxed due to alloying [35]. Furthermore, it has been

89 demonstrated that shell alloying suppressed Auger exciton recombination in core/alloyed shell/

90 shell QDs, thus increasing the PL QY [36].

91 Overcoating a shell layer around the CdS core to improve the PL QY of QDs has rarely been

92 studied. Thus, in this paper, we report on a new strategy to suppress the surface defect states of

93 CdS QDs by coating with a new ternary alloyed shell layer. CdS QDs, characterized by low PL

94 QY due to embedded surface defects were synthesized in this work via the organometallic

95 synthetic route. We have demonstrated for the first time that improved PL QY in CdS QDs can be

96 achieved via passivation with a ternary alloyed AgZnSe shell layer. To the best of our knowledge,

97 our work is the first to overcoat a AgZnSe shell around CdS core QDs with the sole aim of

98 suppressing interfacial defect states in the core QDs. The organic-phase CdS/AgZnSe core/alloyed

99 shell QDs produced in this work hold great promise in light-emitting optoelectronic applications.

100

101 2. Experimental section

102 *2.1. Materials*

103 Cadmium oxide (CdO), myristic acid, trioctylphosphine oxide (TOPO), hexadecylamine (HDA),

104 trioctylphosphine (TOP), octadecene (ODE), oleic acid, sulphur (S), $_L$-cysteine, diethylzinc

105 (Et_2Zn) and zinc oxide (ZnO) were purchased from Sigma Aldrich. Silver nitrate ($AgNO_3$) was

106 purchased from Saarchem. Selenium (Se) was purchased from Merck. Methanol, acetone, hexane

107 and chloroform were purchased from ACE Chemicals.

108

109 *2.2. Characterization*

110 UV/vis absorption spectra were obtained using a Cary Eclipse (Varian) spectrophotometer. PL

111 emission measurements were carried out using a Horiba Jobin Yvon Fluoromax-4

112 spectrofluorometer. Powder X-ray diffraction (PXRD) measurements were determined using a

113 Cu($K\alpha$) radiation (λ=1.54184 Å) on a Bruker D2 Phaser. Transmission electron microscopy (TEM)

114   images were produced using a JEOL JEM 2100F operated at 200 kV. Raman spectra were recorded

115   using a WITec Alpha 300 micro-Raman imaging system with a 488 nm excitation laser and CCD

116   detector at ambient temperature with the laser power below 2 mW in order to reduce heating

117   effects.

118

119   *2.3. Preparation of the precursors*

120   *2.3.1. TOPSe*

121   To prepare the Se precursor, 0.12 g Se was dissolved in 5 mL TOP and sonicated until complete

122   dissolution of Se, thus resulting in a clear solution. The solution was then stirred at room

123   temperature prior to use and was stable for 3 days.

124

125   *2.3.2. TOPZn*

126   To prepare the Zn precursor from Et_2Zn, 1.93 g TOPO was firstly dissolved in 10 mL ODE and 5

127   mL of oleic acid. The solution was then heated up until the complete dissolution of TOPO

128   surfactant, thus resulting in a clear solution. Thereafter, 2 mL Et_2Zn and 1 mL TOP were added

129   and the solution was stirred at room temperature before use.

130   To prepare the Zn precursor from ZnO, 0.4 g ZnO was added to a mixture of 15 mL ODE and 10

131   mL oleic acid and sonicated for a few minutes. Thereafter, the precursor solution was stirred at

132   room temperature prior to use.

133

134   *2.3.3. TOPAg*

135   Ag precursor was prepared by mixing 0.5 g $AgNO_3$ with 5 mL TOP. The solution was then heated

136   up until complete dissolution of the $AgNO_3$ which was evident by the change in colour from

137   colourless to brownish black.

138   *2.3.4. TOPS*

139   To prepare the TOPS precursor used in method 1 synthesis of CdS/AgZnSe QDs (refer to section

140   2.4), 1.93 g TOPO was first dissolved in 15 mL ODE and 10 mL oleic acid followed by the addition

141   of 0.16g S and 1 mL TOP. For method 2 synthesis of CdS/AgZnSe QDs (section 2.5), 1.93 g

142   TOPO was dissolved in 10 mL ODE and 5 mL oleic acid, then 0.08 g S and 1 mL TOP was added

143   thereafter. The solutions were sonicated and heated up to aid complete dissolution of the S and

144   thereafter stirred at room temperature prior to use.

145

146   *2.4. Synthesis of CdS/AgZnSe core/alloyed shell QDs (method 1)*

147   The synthesis of CdS/AgZnSe core/alloyed shell QDs was carried out via the organometallic one-

148   pot synthetic route but with modifications **[37].** Complexation between the Cd ion, surfactants

149   and capping ligands was formed by mixing 1.3 g CdO, 1.2 g myristic acid, 1.93 g TOPO and 1.2

150   g HDA with 50 mL ODE and 30 mL of oleic acid. The solution was bubbled with Ar gas and

151   heated up until complete dissolution of the Cd ion which was evident by a change in colour of the

152   solution from pale brown to colourless. At ~220 °C, TOPS solution was added into the Cd

153   precursor solution to form the CdS core QDs. Once satisfactory growth of the QD core was

154   achieved, a fraction of the growth solution was injected into a beaker. To form the core/alloyed

155   shell QDs, 1 ml of TOPSe solution was added into the CdS growth solution followed swiftly by

156   the addition of 1 mL TOPAg and TOPZn (using ZnO). Portions of the core/shell QDs were taken

157   out at different time intervals.

158 *2.5. Synthesis of CdS/AgZnSe QDs (method 2)*

159 Method 2 synthesis was carried out according to the fabrication steps detailed in method 1 but with

160 slight modifications of the precursor concentrations. For the complexation of Cd ion with the

161 precursor materials, 2 mL TOP, 0.4 g CdO, 0.6 g HDA and 0.6 g myristic acid were mixed with

162 20 mL ODE and 15 mL oleic acid. The synthetic process of method 1 was therefater followed by

163 adding TOPS (prepared specifically for method 2) to form the CdS QDs. Formation of the

164 core/alloyed shell QDs was followed according to method 1 except that TOPZn prepared from

165 ET$_2$Zn was used.

166

3. Results and discussion

168 *3.1. Fabrication of the QDs*

169 One-pot organometallic synthesis of metal precursors in the presence of surfactants, organic-

170 capping ligands and a non-coordinating solvent (ODE) was used to engineer the structure of the

171 QDs. It is well known that the growth kinetics influences the PL emission and absorption evolution

172 of the QDs [38]. The nature of the precursor material with respect to the concentration, quantity,

173 time of injection, temperature and the interplay between them are reaction conditions that influence

174 the growth of the QDs. We have therefore exploited these reaction conditions to engineer the

175 optical properties of CdS/AgZnSe core/alloyed shell QDs.

176 In method 1 synthesis, higher quantities of the Cd metal precursor, surfactants, organic ligands and

177 the non-coordinating solvent were used to aid the Cd-precursor complexation for the subsequent

178 nucleation and growth of CdS QDs. Conversely, lower concentrations of the Cd precursor,

179 surfactants and ligands were employed in method 2 synthesis of the QDs. Before adding the TOPS

180 precursor, the Cd precursor solution was heated up to >200 °C to aid complete dissolution and

181   complexation of the Cd precursor. The change in colour of the solution from brown to colourless

182   confirmed the complexation process which was accompanied by injection of the TOPS precursor.

183   As the CdS core QDs nucleated, the temperature of the growth solution increased steadily and was

184   accompanied by a concomitant change in the colour. During this period, a fraction of the CdS core

185   QDs was removed in order to probe the structural and optical properties thereof in comparison to

186   the core/alloyed shell QDs.

187   The temperature at which the AgZnSe alloyed shell was overcoated on the CdS core surface is

188   very crucial to the overall optical properties of the CdS/AgZnSe core/alloyed shell QDs. At higher

189   temperature and longer reaction time, CdS QDs size distribution is expected to deteriorate and lead

190   to broadening of the spectral line widths. On the other hand, overcoating the shell layer at relatively

191   low temperature could either reduce the crystallinity of CdS/AgZnSe core/alloyed shell QDs or

192   lead to incomplete decomposition of the precursor materials [39]. Therefore, an appropriate

193   temperature was determined independently for each method used to fabricate the core/alloyed shell

194   QDs. The concentration and rate at which the AgZnSe shell precursor is added is also crucial in

195   influencing the optical properties of the QDs. Slow addition of the precursor shell materials

196   prevents homogenous nucleation and induces most of the AgZnSe shell to grow heterogeneously

197   on the CdS nuclei. Hence, the precursor solutions for the shell layering were injected into the CdS

198   growth solution in swift succession. Addition of TOPSe, TOPZn and TOPAg precursors to the

199   CdS growth solution triggered a progressive change in the colour of the solution from orange to

200   red and to dark brown. Different sizes of the CdS/AgZnSe QDs were thereafter harvested at

201   different time intervals whilst the QDs were purified with acetone, chloroform/acetone and

202   chloroform/acetone/ethanol mixture.

203

204 *3.2. Structural properties*

205 *3.2.1. Surface morphology*

206 TEM analysis was used to qualitatively probe the internal structure of the QDs with respect to the

207 shape, size distribution, and shell coverage. Fig. 1A-C shows the TEM images of three different-

208 sized CdS QDs with average sizes of 6.0±0.5, 6.5±0.5 and 7.5±1.2 nm respectively. Our aim was

209 to synthesize uniform-sized CdS QDs in order to effectively understand the structural effects of

210 shell layering. Looking closely at each TEM micrograph, a uniform size distribution, embedded

211 with a mixture of spherical and quasi-spherical shapes was observed. Thus, the monodispersed

212 particle size distribution provides direct indication of homogenous nucleation and growth of the

213 core QDs.

214 Alloyed semiconductor QD nanocrystals can be grouped as having either a gradient internal

215 structure derived from varying the alloy composition or a uniform internal structure ascribed to

216 homogenous alloying. In our work, a fixed composition of the shell precursor was used to engineer

217 the structure of the core/alloyed shell QDs. Fig. 2A-D shows the representative TEM images of

218 CdS/AgZnSe core/alloyed shell QDs synthesized via method 1 with average particle sizes of

219 5.1±0.6, 5.5±0.7, 7.9±1.6 and 9.1±1.9 nm respectively. The striking feature was the decrease in

220 the core/alloyed shell QDs particle size relative to the core which is an unusual phenomenon as

221 the size of the core/shell QDs is expected to increase after shell passivation. Since shell passivation

222 of the 7.5 nm CdS QDs led to rapid nucleation and growth of the different sized CdS/AgZnSe

223 QDs, it is imperative to suggest that either CdS was buried within the shell domain or an

224 intermediate formation of CdS/CdSe occurred before the growth of CdS/AgZnSe QDs.

225 As the CdS/AgZnSe QDs grew, a steady transformation in the particle morphology with respect

226 to the size distribution was observed. The homogeneity of the particle reduced as the size

227 increased, thus indicating that the QDs growth transitioned from an interfacial epitaxial

228 homogenous state to a heterogeneous state. During the period of harvesting each of the different-

229 sized QDs, the temperature of the solution increased from ~240 – 310 °C and this should

230 tentatively influence the nucleation and growth of the QDs. It is also noteworthy to emphasize that

231 the transition in homogeneity of the QDs correlated significantly to the shape engineering of the

232 particle. Looking closely at the TEM monograph of 7.9 nm and 9.1 nm-sized CdS/AgZnSe QDs

233 (Fig. 2C and 2D), the emergence of trigonal-shaped particles was observed. Tentatively, we could

234 attribute the shape engineering of the QDs to the passivating effect of AgZnSe shell, thus implying

235 that the electronic structure of CdS/AgZnSe QDs led to different confinement levels for electron

236 and hole. The hole may be strongly confined to the CdS core while the electron may be delocalised

237 into the shell layer **[40].**

238 Three different sizes of CdS/AgZnSe QDs were harvested using method 2 synthetic route. The

239 corresponding TEM images and particle size histograms are shown in Fig. 3. The particle size

240 distribution revealed a prolate heterogeneous particle morphology, resembling an anisotropic-like

241 growth pattern. The anisotropic growth pattern can be understood in terms of the reaction

242 conditions used in the synthesis as it applies to low reactivity precursors and low volume of

243 coordinating solvent. Under these reaction conditions, CdS/AgZnSe heteroepitaxial growth is

244 kinetically controlled (i.e., AgZnSe formation at the surface is the rate-limiting step, rather than

245 the precursor diffusion) and slow. Thus, the high reactivity of the Ag, Zn and Se of the AgZnSe

246 shell layer will favour anisotropic-type growth **[41].**

247 Generally, the mechanism of nucleation and growth of CdS/AgZnSe QDs can be understood in

248 terms of Ostwald ripening. At relatively low temperature (220–240 °C), Ostwald ripening

249 dominated as a result of dissolution and surface energy of small particles which redissolve to allow

250 subsequent growth of larger particles. At higher temperature (>260 °C), Brownian motion will

251 increase in the synthetic system due to higher thermal energy. Hence it is more likely that the

252 increase in motion will allow the particles to interact at the exact crystallographic orientation,

253 leading to orientated attachment [42].

254

255 *3.2.2. Crystal phase analysis*

256 The crystal structure of CdS core and CdS/AgZnSe QDs was studied using PXRD. From the

257 diffraction pattern of the CdS core (Fig 4), a pure zinc-blende crystal structure with three prominent

258 peaks at planes {111}, {220} and {311} was observed. The three planes exhibited Bragg angles

259 at 26.5°, 43.9° and 51.9° respectively. Comparison of the diffraction pattern of CdS/AgZnSe

260 core/alloyed shell QDs with CdS QDs reveal notable differences. Firstly, the three-notable peaks

261 (associated with zinc-blende crystal structure) present in CdS were observed in $CdS/AgZnSe_{588}$.

262 However, the appearance of four additional peaks between 30–40° and two additional peaks at

263 higher Bragg angle (47.6° and 56.8°) provides direct evidence that the shell alloying process

264 induced crystal phase changes in the QDs. Since the CdS/AgZnSe QDs size was tuned by fixed

265 shell alloying, it is interesting to note the phase transition changes in the core/alloyed shell QDs.

266 As the size of CdS/AgZnSe QDs increased, a steady transformation in the diffraction pattern as it

267 relates to changes in the diffraction peaks was observed. A close assessment of the diffraction

268 pattern of $CdS/AgZnSe_{593}$, revealed detailed formation of a duplet peak at low Bragg angle which

269 can be attributed to the steady phase transition from a zinc-blende diffraction pattern to a wurtzite

270 diffraction pattern. Further growth of the core/alloyed shell QDs led to the formation of a triplet

271 peak at low angle as observed from the diffraction pattern of $CdS/AgZnSe_{599}$. Further assessment

272 of the diffraction pattern of $CdS/AgZnSe_{601}$ revealed the formation of a pure wurtzite diffraction

273 pattern. Thus, is can be concluded that CdS core QDs favoured a zinc-blende crystal structure

274 while the CdS/AgZnSe core-alloyed QDs kinetically favoured a phase change from a zinc-blende

275 diffraction pattern to a wurtzite diffraction pattern.

276

277 *3.2.3. Raman analysis*

278 Core/shell QDs have been proven to reduce Auger recombination rates, which is important in

279 multiexciton recombination and OFF/ON blinking process **[43].** It is also believed that the

280 core/shell interfacial alloying region is associated with a graded interface **[44].** Hence, the potential

281 of Raman to probe the internal structure of the core/alloyed shell QDs interface was investigated.

282 Fig. 5 shows the Raman spectra for CdS core and the different-sized CdS/AgZnSe QDs. The

283 similarities with reference to the peak position of CdS longitudinal optical phonon (LO) bulk

284 frequency at ~ 300 cm^{-1} and CdS overtone at ~ 600 cm^{-1} with those of CdS/AgZnSe$_{588}$ and

285 CdS/AgZnSe$_{93}$, provides strong indication of the homogenous growth of the core/alloyed shell

286 QDs. For CdS/AgZnSe$_{599}$ and CdS/AgZnSe$_{601}$, we observed significant changes in the peak

287 position when compared to the CdS core. Specifically, the peak position of CdS/AgZnSe$_{599}$

288 exhibited similar frequency to CdS LO frequency but the peak at the CdS overtone region was

289 more blue-shifted in frequency. Conversely, the peak frequencies of CdS/AgZnSe$_{599}$ relative to

290 CdS LO and the overtone region were more red-shifted in comparison to the CdS core. The degree

291 of frequency shift in CdS/AgZnSe$_{599}$ and CdS/AgZnSe$_{601}$ peak position relative to CdS can be

292 understood in terms of the growth morphology and the degree of interfacial defect states in the

293 QDs. Thus, the frequency shift and strain relaxation in the core/alloyed shell interface will differ

294 due to the QDs size and shell thickness. The relatively less-pronounced peaks below 220 cm^{-1} for

295 the core/alloyed shell QDs can be ascribed to a surface optical phonon feature which is inherent in

296 finite sized crystals and also from the varying degree of alloying at the interface between CdS core

297 and AgZnSe shell **[45,46]**. The variation in the intensity of the modes below 220 cm^{-1} could

298 probably also account for the differences in alloying efficiency of the AgZnSe shell relative to the

299 CdS core.

300

301 *3.3. Optical properties*

302 The QDs surface is influenced by the nature and chemical reaction of the synthetic constituents

303 (surfactants, capping ligands and solvents) used in fabricating its structure. The atomistic effects

304 of these constituents form the basis for assessing the quality of the QDs surface as it relates to the

305 optical properties, such as the PL stability, spectral features and PL QY. The formation of midgap,

306 deep and shallow states as surface traps provides the basis to which nonradiative electron-hole

307 recombination degrades the QDs fluorescence. The suppression or total elimination of surface trap

308 states in core QDs via coating of a shell layer is useful for light-associated applications and it

309 provides a platform for better understanding of synthetic fabrication strategies required to

310 construct high-quality QD nanocrystals. Our objective is to investigate the influence of a new shell

311 layer (AgZnSe) on the luminescent properties of colloidal CdS QDs. We have utilized the shell

312 alloying process to unravel how the QDs band gap and synthetic fabrication strategy influences

313 the PL properties of CdS/AgZnSe core/alloyed shell QDs. The PL QY was determined according

314 to the equation:

315

316 $$\Phi_F^{QD} = \Phi_F^{Std} \frac{F_{QDs}.OD_{Std(\lambda exc)}.n^2_{water}}{F_{Std.}OD_{QD_{(\lambda exc)}}.n^2_{ethanol}}$$ (1)

317

318   Where Φ_F^{Std} is the PL quantum yield of rhodamine 6G standard in ethanol ($\Phi = 0.95$); F_{Std} and F_{QDs}

319   are the integrated sum of the fluorescence intensity of the standard and QDs; $OD_{QD_{(\lambda exc)}}$ and $OD_{Std(\lambda exc)}$

320   are the optical densities of the QDs and standard while $n_{ethanol}^2$ and $n^2{}_{water}$ are the refractive indices of

321   ethanol and water used to prepare the standard and QDs respectively.

322   Fig. 6A and B shows the evolution of the PL emission and absorption spectra of three different-

323   sized CdS core QDs and Table 1 summarizes the corresponding photophysical properties as they

324   relate to the absorption wavelength maximum, full width at half maximum (FWHM), band gap

325   and PL QY. We harvested three-sized CdS core QDs with the sole aim of assessing their optical

326   properties in comparison to the different-sized CdS/AgZnSe core/alloyed shell QDs. A small red

327   shift in PL emission was observed for the harvested different-sized CdS core QDs with the

328   absorption wavelength maximum and FWHM increasing in relation to the core size. The striking

329   feature is the low PL QY which was increasingly tuned from 4 to 16% and also dependent on each

330   core size. We observed that CdS_{471} produced the highest PL QY of 16% while the lowest PL QY

331   value of 4% was exhibited by CdS_{478}. Based on the relatively low PL QY, CdS core QDs suffers

332   significantly from interfacial surface defects and residual strain in which the degree of defect states

333   depends on the core size.

334   To effectively understand the effect of ternary AgZnSe shell alloying on the PL properties of CdS

335   QDs, we employed two synthetic fabrication strategies. The most obvious and direct evidence of

336   shell alloying comes from the PL emission and absorption spectra shown in Fig. 6C. The evolution

337   of the PL emission of CdS/AgZnSe QDs synthesized via method 1 was tuned from 588 to 601 nm

338   while the absorption spectra (Fig. 6D) was tuned from 464 nm to 477 nm. AgZnSe shell precursors

339   used in method 1 synthesis of CdS/AgZnSe QDs was added into the growth solution after

340   harvesting fraction of CdS_{481} core QDs. The striking feature is the blue-shifted absorption

341   wavelength and corresponding red shift in PL emission of CdS/AgZnSe$_{588}$ relative to CdS$_{481}$ QDs.

342   The shift reveals that the shell alloying strategy, induced bad gap modulation of the QDs in the

343   visible region of the electromagnetic spectrum. For CdS/AgZnSe QDs synthesized via method 2,

344   the PL emission spectra was tuned from 591 to 612 nm (Fig. 7A) while the absorption spectra were

345   tuned from 449 to 481 (Fig. 7B). Despite the PL emission being more red-shifted relative to the

346   CdS core, the absorption spectrum of CdS/AgZnSe$_{591}$ was significantly blue-shifted. From Table

347   1, the efficiency of band gap modulation of CdS/AgZnSe QDs was observed to vary narrowly

348   from 2.07–2.11 eV for method 1 synthesis and from 2.03–2.10 eV for method 2 synthesis of the

349   QDs.

350   To determine if the band gap modulation of CdS/AgZnSe QDs originated from the intrinsic optical

351   properties of the core/alloyed nanostructures, a deeper assessment of the PL QY values (Table 1)

352   was performed. The most striking observation is the variation in the PL QY of CdS/AgZnSe QDs

353   synthesized via method 1 and 2 and the remarkable increase in comparison to the values obtained

354   for CdS core. Via method 1 synthesis, the PL QY of CdS/AgZnSe QDs was tuned from 48 to 51%

355   but via method 2 synthesis the PL QY was tuned from 35 to 73%. It is noteworthy that shell

356   alloying of CdS QDs suppressed interfacial defect states in the core/alloyed shell nanocrystals due

357   to the remarkable increase in the PL QY. However, it is important to emphasize that the defect

358   state suppression efficiency varied amongst the QDs size and was dependent on the quality of the

359   fabrication method.

360   Examining closely how the shell alloying process influenced the optical properties of the QDs, we

361   have probed the correlation between the band gap modulation and the PL QY. It is a well-

362   established phenomenon that a semiconductor band gap can be reduced by residual strain, thus

363   leading to deformed potential **[47,48].** Therefore, the low PL QY reveals that CdS core QDs suffer

364   from residual strain due to surface traps embedded within the nanocrystals. The narrow band gap

365   (2.07–2.11 eV) exhibited by the different-sized CdS/AgZnSe QDs (synthesized via method 1),

366   correlated precisely to the small difference in PL QY (48-51%). This suggests that suppression of

367   surface defect states in CdS QDs was with a very small margin across the core/alloyed shell QDs

368   size. However, a wider margin in defect state suppression was observed for CdS/AgZnSe QDs

369   synthesized via method 2, due to the wider difference in PL QY from 35% to 73%. Two important

370   features are the maximum PL QY of 73% and the precise correlation in the margin of difference

371   between the band gap and the PL QY. It is also noteworthy that the high PL QY implies much of

372   the surface defects were suppressed by the shell alloying process while the variation in PL QY

373   correlated precisely to the efficiency of surface defect suppression.

374

375   **4. Conclusions**

376   The passivation of CdS QDs with a new ternary alloyed AgZnSe shell layer was obtained via the

377   organometallic synthetic route. The band gap of CdS/AgZnSe core/alloyed shell QDs was tuned

378   across the visible region with the nanocrystals exhibiting varying PL QYs. We observed a precise

379   correlation in the margin of difference between the band gap of the QDs and the PL QY. The effect

380   of shell alloying was observed in the QDs growth morphology in which the QDs growth

381   transitioned from a homogeneous state to a heterogeneous state. Transition in the phase structure

382   of the QDs from a zinc blende diffraction pattern to a wurtzite diffraction pattern was also

383   observed. Generally, we have established that AgZnSe shell passivation on luminescent CdS QDs

384   suppressed interfacial defect states in the CdS core QDs with the degree of suppression dependent

385   on the size of the QDs derived from the finely-tuned synthetic fabrication strategy.

386

Reference

[1] T.V. Duncan, M.A. Mendez Polanco, Y. Kim and S.-J. Park, Improving the quantum yields of semiconductor quantum dots through photoenhancement assisted by reducing agents, J. Phys. Chem. C, 11 (2009) 7561−7566.

[2] A. Hassinen, I. Moreels, K. De Nolf, P.F. Smet, J.C. Martins and Z. Hens, Short-chain alcohols strip X-type ligands and quench the luminescence of PbSe and CdSe Quantum dots, acetonitrile does not, J. Am. Chem. Soc. 134 (2012) 20705−20712.

[3] M. Nasilowski, P. Spinicelli, G. Patriarche, B. Dubertret, Gradient CdSe/CdS quantum dots with room temperature biexciton unity quantum yield, Nano Lett. 15 (2015) 3953−3958.

[4] P. Reiss, M. Protière, L. Li, Core/shell semiconductor nanocrystals, Small 5 (2009) 154−168.

[5] D.V. Talapin, J.-S. Lee, M.V. Kovalenko, E.V. Shevchenko, Prospects of colloidal nanocrystals for electronic and optoelectronic applications. Chem. Rev. 110 (2010) 389−458.

[6] O. Chen, J. Zhao, V.P. Chauhan, J. Cui, C. Wong, D.K. Harris, H. Wei, H.-S. Han, D. Fukumura, R.K. Jain, M.G. Bawendi, Compact high-quality CdSe−CdS core−shell nanocrystals with narrow emission linewidths and suppressed blinking. Nat. Mater. 12 (2013) 445−451.

[7] C. Giansante, I. Infante, Surface traps in colloidal quantum dots: a combined experimental and theoretical perspective, J. Phys. Chem. Lett. 8 (2017) 5209−5215.

409 [8] M. Nirmal, B.O. Dabbousi, M.G. Bawendi, J.J. Macklin, J.K. Trautman, T.D. Harris, L.E.

410 Brus, Fluorescence intermittency in single cadmium selenide nanocrystals, Nature 383 (1996)

411 802−804.

412 [9] A. Efros, M. Rosen, Random telegraph signal in the photoluminescence intensity of a single

413 quantum dot, Phys. Rev. Lett. 78 (1997) 1110−1113.

414 [10] Y. Altintas, M.Y. Talpur, M. Ünlü, E. Mutlugün, Highly efficient cd-free alloyed core/shell

415 quantum dots with optimized precursor concentrations, J. Phys. Chem. C 120 (2016)

416 7885−7892.

417 [11] J. Bang, J. Park, J.H. Lee, N. Won, J. Nam, J. Lim, B.Y. Chang, H.J. Lee, B. Vhon, J. Shin,

418 J.B. Park, .H. Choi, K. Cho, S.M. Park, T. Joo, S. Kim, ZnTe/ZnSe (core/shell) type-ii quantum

419 dots: their optical and photovoltaic properties, Chem. Mater. 22 (2010) 233–240.

420 [12] M.D. Tessier, D. Dupont, K. De Nolf, J. De Roo, Z. Hens, Economic and Size-tunable

421 synthesis of InP/ZnE (E = S, Se) colloidal quantum dots, Chem. Mater. 27 (2015) 4893−4898.

422 [13] W. Jiang, A. Singhal, J. Zheng, C. Wang, W.C.W. Chan, Optimizing the synthesis of red-

423 to near-ir-emitting CdS-capped $CdTe_xSe_{1-x}$ alloyed quantum dots for biomedical imaging,

424 Chem. Mater. 18 (2006) 4845-4854.

425 [14] P. Tyagi, P. Kambhampati, Independent control of electron and hole localization in

426 core/barrier/shell nanostructures, J. Phys. Chem. C, 116 (2012) 8154–8160.

427 [15] M. Nasilowski, P. Spinicelli, G. Patriarche, B. Dubertret, Gradient CdSe/CdS quantum dots

428 with room temperature biexciton unity quantum yield. Nano Lett. 15 (2015) 3953−3958.

429 [16] M. Wang, M. Zhang, J. Qian, F. Zhao, L. Shen, G.D. Scholes, M.A. Winnik, Enhancing

430 the photoluminescence of polymer-stabilized CdSe/CdS/ZnS core/shell/shell and CdSe/ZnS

core/shell quantum dots in water through a chemical-activation approach, Langmuir 25 (2009) 11732–11740.

[17]   W. Liu, H. Soo Choi, J.P. Zimmer, E. Tanaka, J.V. Frangioni, M. Bawendi, Compact cysteine-coated CdSe(ZnCdS) quantum dots for in vivo applications, J. Am. Chem. Soc. 129 (2007) 14530-14531.

[18]   K. Yu, S. Singh, N. Patrito, V. Chu, Effect of reaction media on the growth and photoluminescence of colloidal CdSe nanocrystals, Langmuir 20 (2004) 11161-11168.

[19]   R.E. Bailey, S. Nie, Alloyed semiconductor quantum dots: tuning the optical properties without changing the particle size, J. Am. Chem. Soc. 125 (2003) 7100-7106.

[20]   J. Quyang, C.I. Ratcliffe, D. Kingston, B. Wilkinson, J. Kuijper, X. Wu, J.A. Ripmeester, K. Yu, Gradiently alloyed $Zn_xCd_{1-x}S$ colloidal photoluminescent quantum dots synthesized via a noninjection one-pot approach, J. Phys. Chem. C 112 (2008) 4908-4919.

[21]   R. Gui, A. Wan, H. Jin, H. Li, C. Zhou, Acetyl acetonate-stabilized $Mn2^+$:CdS quantum dots: Aqueous synthesis and reversible fluorescence tuned by redox reaction, Mater. Lett. 98 (2013) 190-193.

[22]   R. Gui, X. An, H. Su, W. Shen, Z. Chen, X. Wang, A near-infrared-emitting CdTe/CdS core/shell quantum dots-based OFF–ON fluorescence sensor for highly selective and sensitive detection of $Cd2^+$, Talanta 94 (2012) 257-262.

[23]   R. Gui, X. An, Layer-by-layer aqueous synthesis, characterization and fluorescence properties of type-II CdTe/CdS core/shell quantum dots with near-infrared emission. RSC Adv. 3 (2013) 20959-20969.

[24]   M.V. Rama Krishna, R.A. Friesner, Quantum confinement effects in semiconductor clusters, J. Chem. Phys. 95 (1991) 8309-8322.

[25]   I. Hernandez-Calderon, II-VI Semiconductor Materials and Their Applications, (Ed. Tamargo, M. C.), P136-138, Vol. 12 in Optoelectronic Properties of Semiconductors and Superlattices; Manasreh, M. O., Ed.; Taylor & Francis Inc.: New York, 2002.

[26]   A. I. Ekimov, I. A. Kudryavtsev, M. G. Ivanov, A.L. Efros, Spectra and decay kinetics of radiative recombination in CdS microcrystals, J. Lumin. 46 (1990) 83-95.

[27]   K. Gong, D.F. Kelley, Lattice strain limit for uniform shell deposition in zincblende CdSe/CdS quantum dots, J. Phys. Chem. Lett. 6 (2015) 1559−1562.

[28]   C.-C. Hung, S.-J. Ho, C.-W. Yeh, G.-H. Chen, J.-H. Huang, H.-S. Chen, Highly luminescent dual-color–emitting alloyed [$Zn_xCd_{1−x}Se_yS_{1−y}$] quantum dots: investigation of bimodal growth and application to lighting, J. Phys. Chem. C 121 (2017) 28373−28384.

[29]   L.A. Swafford, L.A. Weigand, M.J. Bowers, J.R. McBride, J.L. Rapaport, T.L. Watt, S.K. Dixit, L.C. Feldman, S.J. Rosenthal, Homogeneously alloyed CdS_xSe_{1-x} nanocrystals: synthesis, characterization, and composition/size-dependent band gap, J. Am. Chem. Soc. 128 (2006) 12299.

[30]   Z. Pan, K. Zhao, J. Wang, H. Zhang, YY. Feng, X. Zhong, Near infrared absorption of $CdSe_xTe_{1−x}$ alloyed quantum dot sensitized solar cells with more than 6% efficiency and high stability, ACS Nano 7 (2013) 5215–5222.

[31]   A. Kigel, M. Brumer, A. Sashchiuk, L. Amirav, E. Lifshitz, $PbSe/PbSe_xS_{1-x}$ core-alloyed shell nanocrystals, Mater. Sci. Eng., C 25 (2005) 604-608.

[32]   H. Jin, R. Gui, Z. Wang, J. Xia, M. Yang, F. Zhang, S. Bi, Facile fabrication of water-dispersible $AgInS_2$ quantum dots and mesoporous $AgInS_2$ nanospheres with visible photoluminescence, RSC Adv. 5 (2015) 68287-68292.

476   [33]   P. Yang, M. Ando, N. Murase, Highly luminescent CdSe/Cd$_x$Zn$_{1-x}$S quantum dots coated

477   with thickness-controlled SiO$_2$ shell through silanization, Langmuir 27 (2011) 9535–9540.

478   [34]   K. Boldt, N. Kirkwood, G.A. Beane, P. Mulvaney, Synthesis of highly luminescent and

479   photo-stable, graded shell CdSe/Cd$_x$Zn$_{1-x}$S nanoparticles by in situ alloying, Chem. Mater. 25

480   (2013) 4731−4738.

481   [35]   S.M. Fairclough, E.J. Tyrrell, D.M. Graham, P.J.B. Lunt, S.J.O. Hardman, A. Pietzsch, F.

482   Hennies, J. Moghal, W.R. Flavell, A.A.R. Watt, J.M.J. Smith, Growth and characterization of

483   strained and alloyed Type-II ZnTe/ZnSe core–shell nanocrystals, Phys. Chem. C 16 (2012)

484   26898−26907.

485   [36]   W.K. Bae, L.A. Padilha, Y.-S. Park, H. McDaniel, I. Robel, J.M. Pietryga, V.I. Klimov,

486   Controlled alloying of the core-shell interface in CdSe/CdS quantum dots for suppression of

487   Auger recombination, ACS Nano 7 (2013) 3411−3419.

488   [37]   O. Adegoke, K. Takemura, E.Y. Park, Plasmonic oleylamine-capped gold and silver

489   nanoparticle-assisted synthesis of luminescent alloyed CdZnSeS quantum dots, ACS Omega 3

490   (2018) 135-1366.

491   [38]   J. Quyang, C.I. Ratcliffe, D. Kingston, B. Wilkinson, J. Kuijper, X. Wu, J.A. Ripmeester,

492   K. Yu, Gradiently alloyed Zn$_x$Cd$_{1-x}$S colloidal photoluminescent quantum dots synthesized via

493   a noninjection one-pot approach, J. Phys. Chem. C 112 (2008) 4908-4919.

494   [39]   B.O. Dabbousi, . Rodriguez-Viejo, F.V. Mikulec, J.R. Heine, H. Mattoussi, R. Ober, K.F.

495   Jensen, M.G. Bawendi, (CdSe)ZnS core-shell quantum dots: synthesis and characterization of

496   a size series of highly luminescent nanocrystallites, J. Phys. Chem. B 101 (1997) 9463-9475.

497   [40]   D.V. Talapin, I. Mekis, S. Götzinger, A. Kornowski, O. Benson, H. Weller, CdSe/CdS/ZnS

498   and CdSe/ZnSe/ZnS core-shell-shell nanocrystals, J. Phys. Chem. B 108 (2004) 18826-18831.

499   [41]   P.T.K. Chin, C. de Mello Donega, S.S. van Bavel, S.C.J. Meskers, N.AJ.M. Sommerdijk,

500   R.A.J. Janssen, Highly luminescent CdTe/CdSe colloidal heteronanocrystals with temperature-

501   dependent emission color, J. Am. Chem. Soc. 129 (2007) 14880-14886.

502   [42]   N.T.K. Thanh, N. Maclean, S. Mahiddine, Mechanisms of nucleation and growth of

503   nanoparticles in solution, Chem. Rev. 114 (2014) 7610−7630.

504   [43]   F.; Garcia-Santamaría, S. Brovelli, R. Viswanatha, J.A. Hollingsworth, H. Htoon, S.A.

505   Crooker, V.I. Klimov, Breakdown of volume scaling in Auger recombination in CdSe/CdS

506   heteronanocrystals: the role of the core-shell interface, Nano Lett. 11 (2011) 687−693.

507   [44]   G.E. Cragg, A.L. Efros, Suppression of auger processes in confined structures, Nano Lett.

508   10 (2009) 313−317.

509   [45]   F. Comas, N. Studart, G.E. Marques, Optical phonons in semiconductor quantum rods,

510   Solid State Commun. 130 (2004) 477−480.

511   [46]   H. Lange, M. Artemyev, U. Woggon, C. Thomsen, Geometry dependence of the phonon

512   modes in CdSe nanorods, Nanotechnology 20 (2009) 045705.

513   [47]   J. Kim, M.V. Fischetti, Electronic band structure calculations for biaxially strained Si, Ge,

514   and III-V Semiconductors. J. Appl. Phys. 108 (2010) 013710.

515   [48]   J. Kim, M.V. Fischetti, S. Aboud, Structural, electronic, and transport properties of silicane

516   nanoribbons. Phys. Rev. B 86 (2012) 205323.

517

518

519

520

521

522   **Table 1.** Summary of the photophysical properties of the different-sized CdS core and

523   CdS/AgZnSe QDs.

QDs-λ_{Emi} (nm)	λ_{Abs} (nm)	FWHM (nm)	Band gap (eV)	PL QY (%)
CdS$_{471}$	458	20	2.64	16
CdS$_{478}$	471	26	2.60	4
CdS$_{481}$	476	33	2.58	8
[a]CdS/AgZnSe$_{588}$	464	41	2.11	48
[b]CdS/AgZnSe$_{591}$	449	34	2.10	73
[a]CdS/AgZnSe$_{593}$	468	42	~2.10	50
[a]CdS/AgZnSe$_{599}$	473	40	2.07	49
[a]CdS/AgZnSe$_{601}$	477	45	~2.07	51
[b]CdS/AgZnSe$_{602}$	473	39	2.06	35
[b]CdS/AgZnSe$_{612}$	481	40	2.03	42

524   [a] Method 1 synthesis

525   [b] Method 2 synthesis

526

527

528

529

530

531

532

533

534
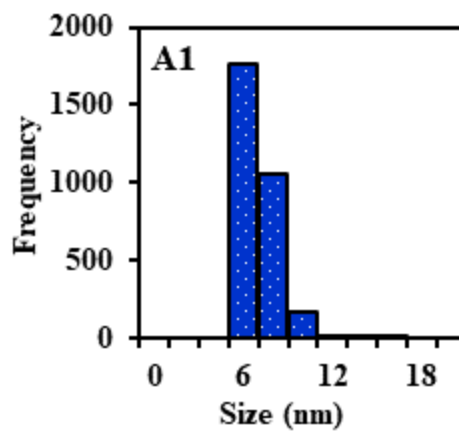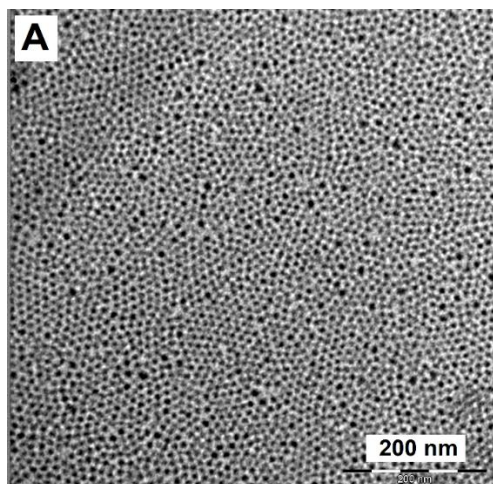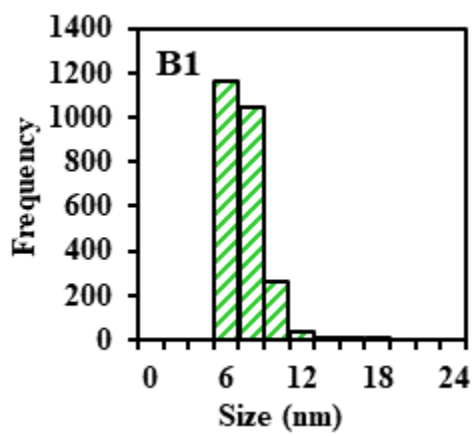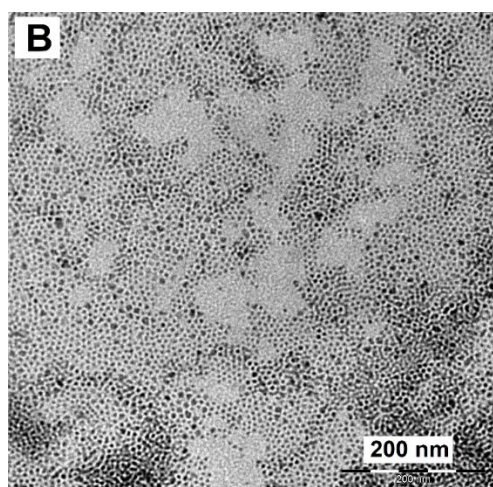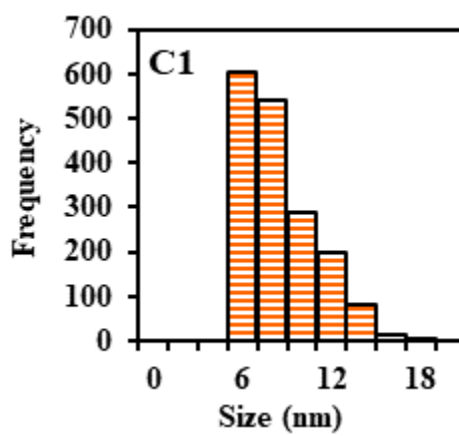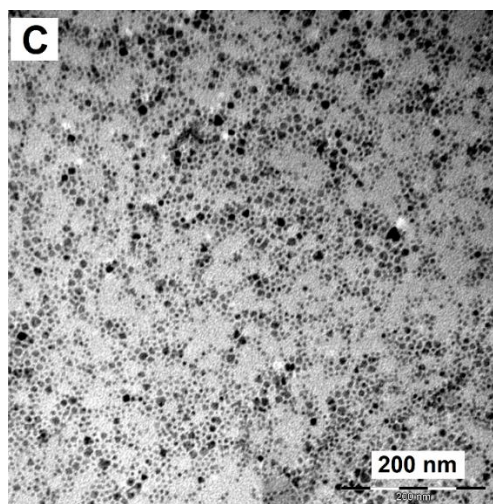
Fig. 1. TEM images (A, B and C) and average particle size distribution (A1, B1 and C1) of CdS

core QDs.

537

538

539

540

541
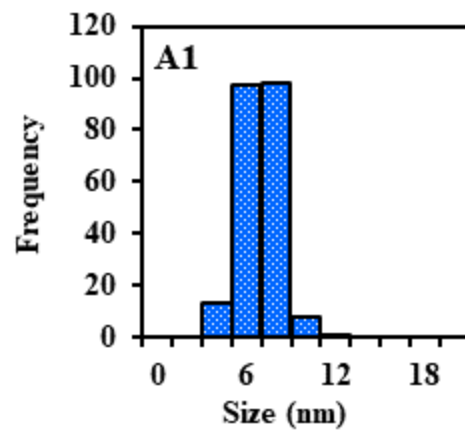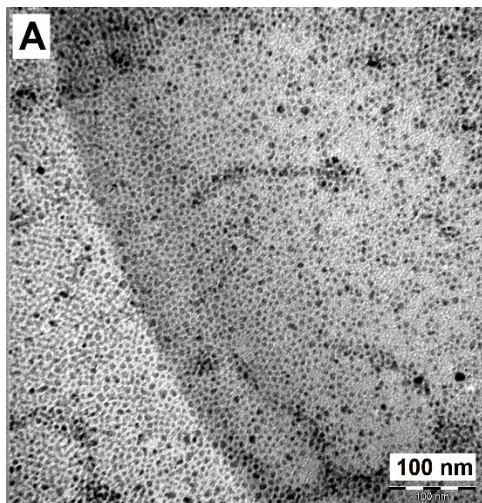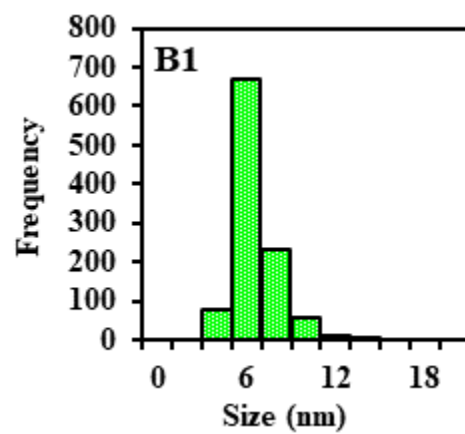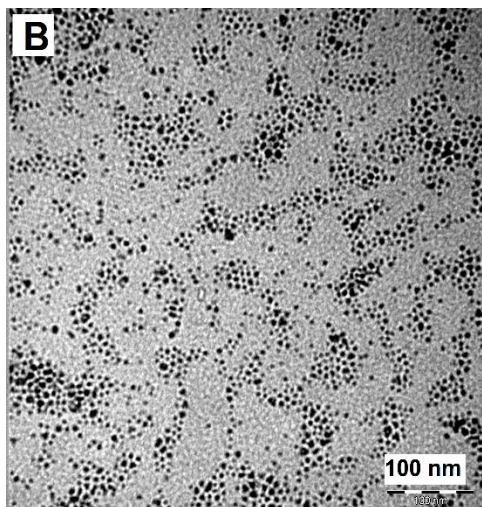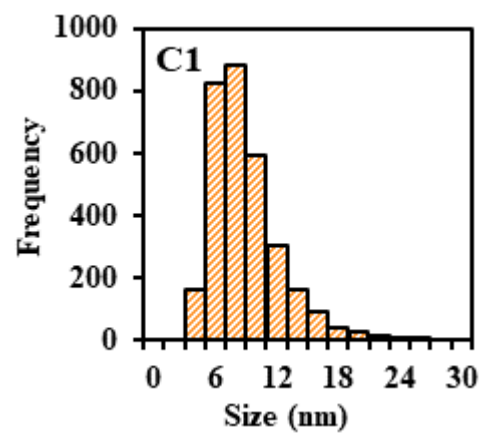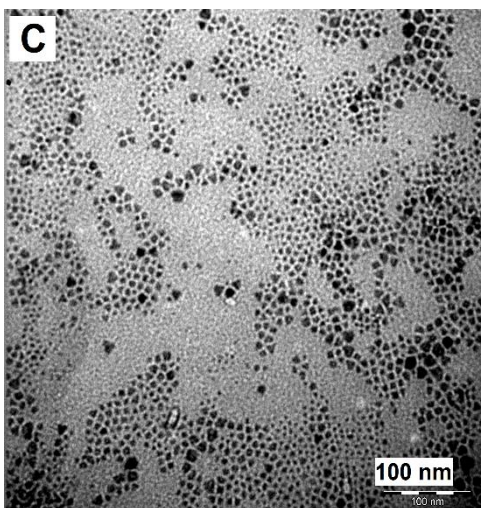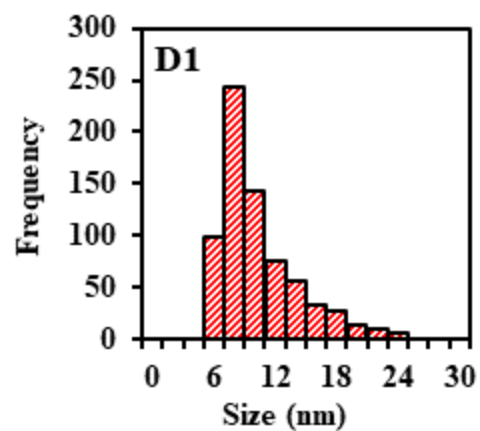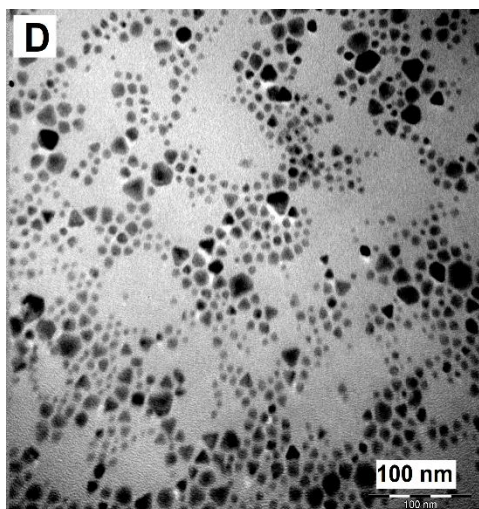
Fig. 2. TEM images (A, B, C and D) and average particle size distribution (A1, B1, C1 and D1)

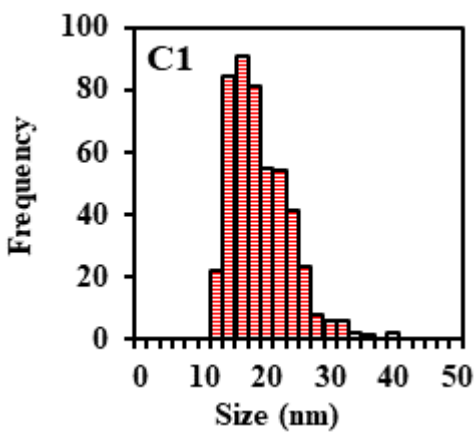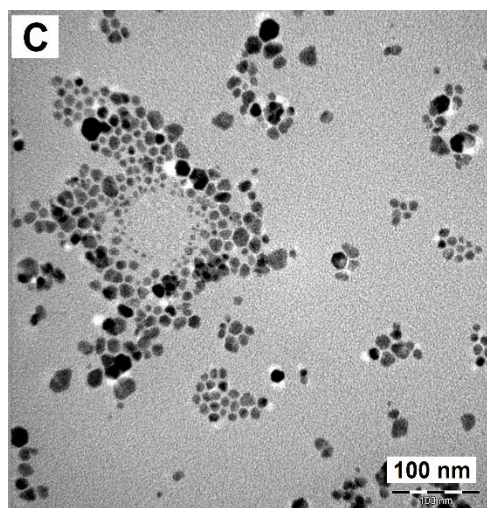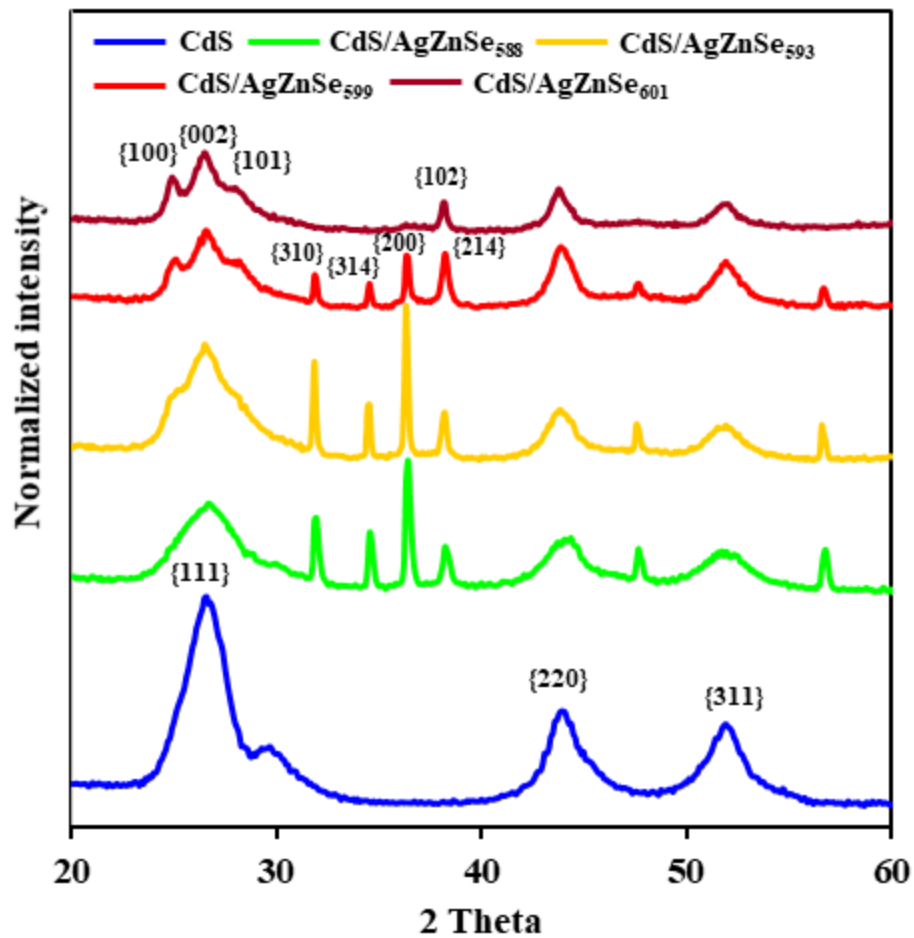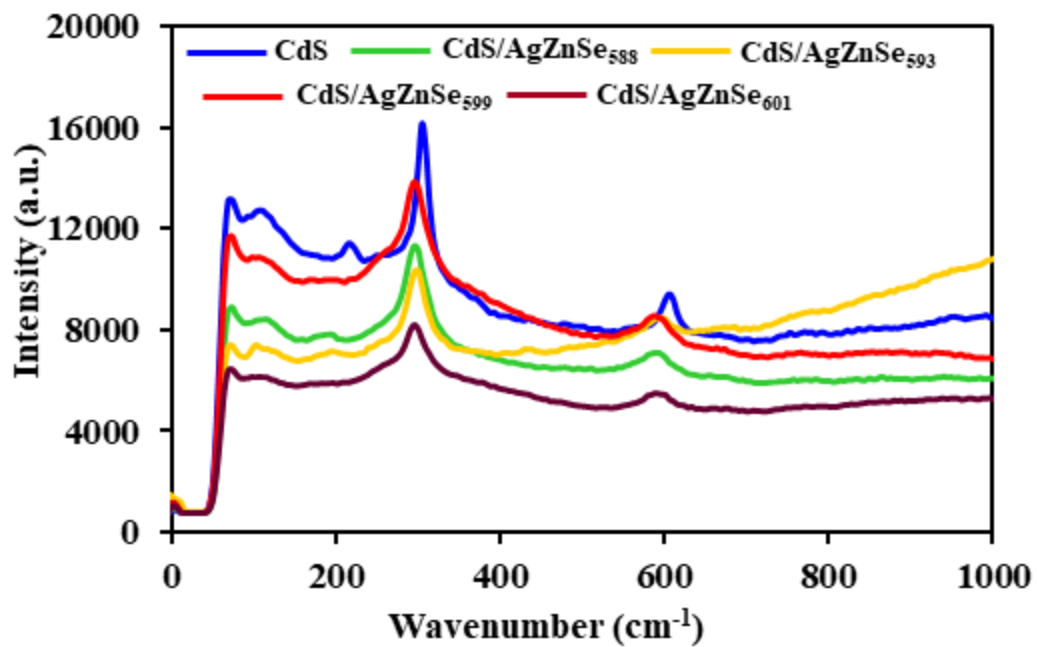of CdS/AgZnSe core/alloyed shell QDs synthesized via method 1.

556
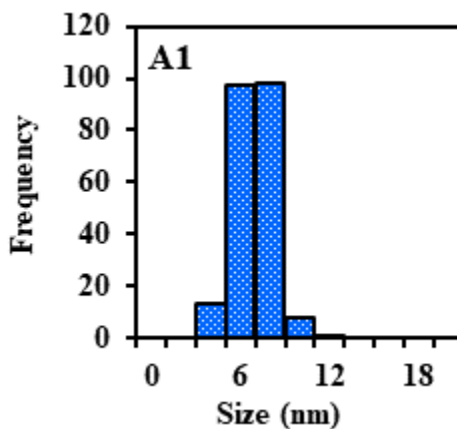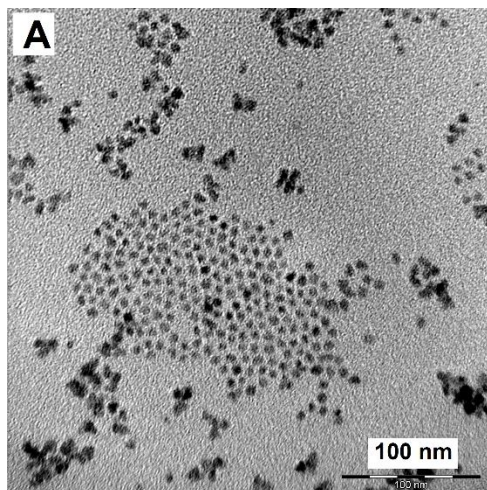
557
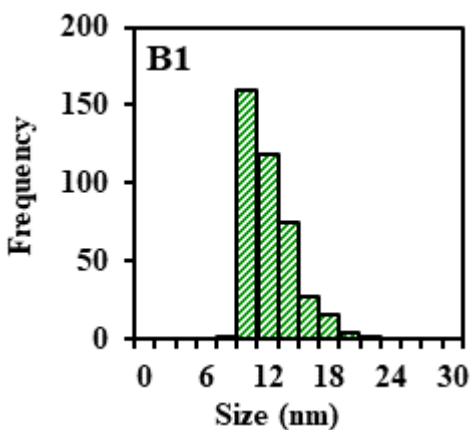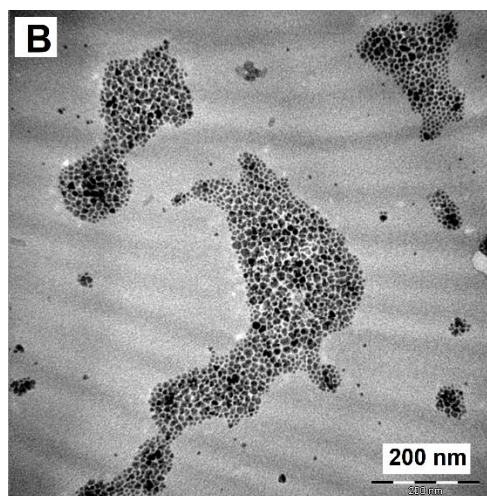
558

559 **Fig. 3.** TEM images (A, B and C) and average particle size distribution (A1, B1 and C1) of

560 CdS/AgZnSe core/alloyed shell QDs synthesized via method 2.

Fig. 4. PXRD plots of CdS, CdS/AgZnSe$_{588}$, CdS/AgZnSe$_{593}$, CdS/AgZnSe$_{599}$ and CdS/AgZnS$_{601}$ QDs.

572

Fig. 5. Raman spectra of CdS, CdS/AgZnSe$_{588}$, CdS/AgZnSe$_{593}$, CdS/AgZnSe$_{599}$ and
CdSe/AgZnS$_{601}$ QDs.
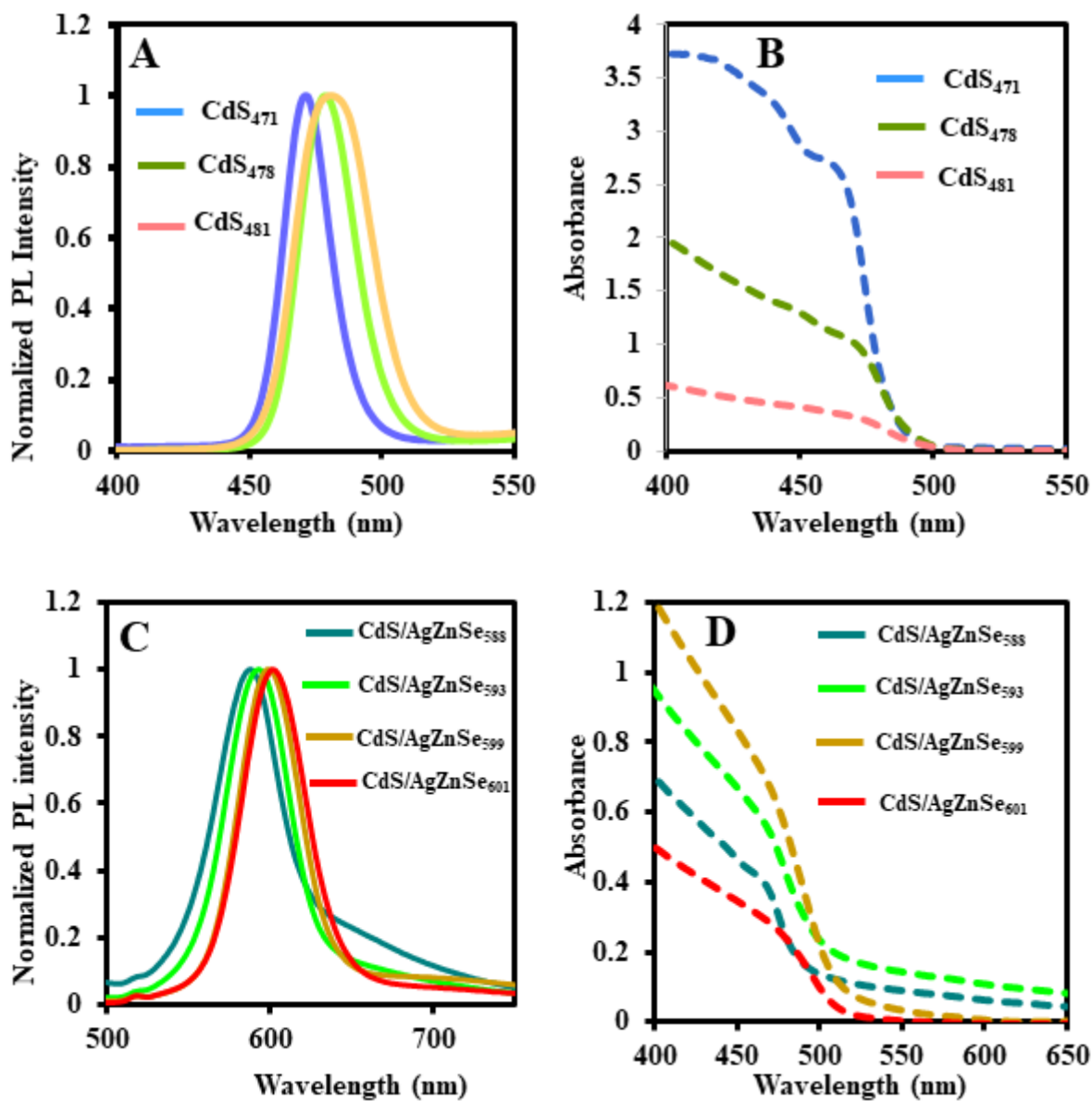
581

582

Fig. 6. PL and UV/vis absorption spectra of the different sized CdS (A and B) and CdS/AgZnSe

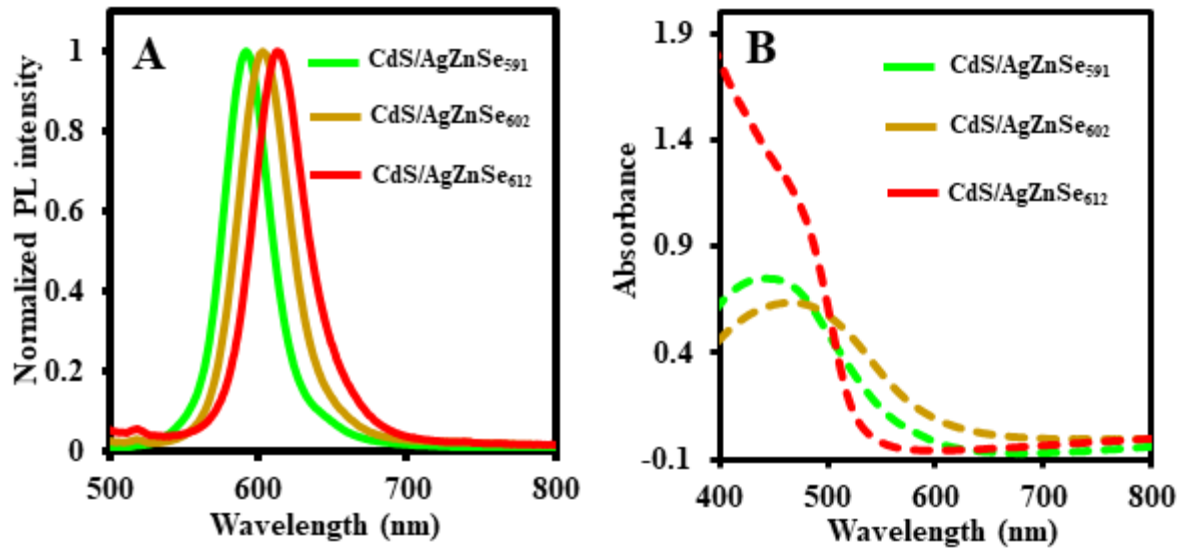core/alloyed shell QDs (C and D) synthesized via method 1.

585

586

587

588

589

Fig. 7. PL (A) and UV/vis absorption (B) spectra of the different sized and CdS/AgZnSe core/alloyed shell QDs synthesized via method 2.